Nanoscale Manipulation of Pyrochlore: New Nanocomposite Ionic Conductors

J. Lian,[1] L. M. Wang,[1] S. X. Wang,[1] J. Chen,[1] L. A. Boatner,[2] and R. C. Ewing[1,3,*]

[1]*Department of Nuclear Engineering & Radiological Sciences, University of Michigan, Ann Arbor, Michigan 48109-2104*

[2]*Solid State Division, Oak Ridge National Laboratory, Oak Ridge, Tennessee 37831-6056*

[3]*Department of Materials Science & Engineering, University of Michigan, Ann Arbor, Michigan 48109-2104*

(Received 8 May 2001; published 17 September 2001)

The ionic conductivity of isometric pyrochlore, ideally $A_2B_2O_7$, is extremely sensitive to disordering of A- and B-site cations and oxygen anion vacancies. We report the first use of ion beam irradiation-induced disordering in $Gd_2Ti_2O_7$ to produce a strain-free, buried, disordered defect-fluorite layer approximately 12 nm thick within an ordered pyrochlore matrix. This approach provides a new means of creating nanoscale, mixed ionic-electronic conductors in pyrochlore ceramics, such as those required for solid-state electrochemical cells.

DOI: 10.1103/PhysRevLett.87.145901 PACS numbers: 81.07.–b, 61.80.Jh, 68.37.Lp, 81.40.–z

The effects of cation and anion disordering on the conductivity of pyrochlore inspired us to attempt to use ion-beam irradiation to fabricate nanoscale microstructures by controlling the degree of disorder so as to alter the electronic/ionic conduction properties of pyrochlore materials. It is the extremely wide range in electronic properties combined with the extreme differences in response to radiation damage in the $Gd_2(Zr_xTi_{1-x})_2O_7$ binary system that holds such great promise for designing new functional materials.

Pyrochlore materials, $A_{1-2}B_2O_6Y_{0-1}$, encompass a wide range of chemistry that is manifest in over 450 synthetic compositions [1,2]. The diverse chemistry is coupled to a remarkable variation of properties that is important in numerous technological applications such as catalysis, piezoelectricity, ferro- and ferrimagnetism, luminescence, giant magnetoresistance, and resistance to radiation damage. The electronic properties vary from being metallic or semiconducting to having a high ionic conductivity [1,3,4]. Pyrochlore materials are a derivative of the fluorite structure, AX_2, but with two cation sites and one-eighth fewer anions [1,2] (Fig. 1). Most pyrochlores have III-IV compositions with the formula $A_2^{3+}B_2^{4+}O_7$. The atomic arrangement is completely specified except for the x positional parameter for the $48f$ oxygen, which defines the displacement from the ideal fluorite structure. The ordered pyrochlore structure becomes disordered at high temperatures (e.g., 1530 °C for $Gd_2Zr_2O_7$) [5], as is evidenced by the loss of intensity of the supercell diffraction maxima and a halving of the unit cell parameter. Disorder may also be introduced by compositional changes, such as the substitution of Zr for Ti. As the cation size of the A and B site becomes more similar, disordering is introduced. The pyrochlore structure is unusual among oxides in that the order/disorder transition must occur on both the cation and anion lattices.

Variations in the ionic and electronic conductivity of pyrochlore compounds, $A_2B_2O_7$, are related to disordering of the A- and B-site cations and the oxygen anion vacancies [3,6–8]. The $Gd_2(Zr_xTi_{1-x})_2O_7$ pyrochlore is an extrinsic ionic conductor [9] at low values of x, but it becomes an intrinsic fast-ion conductor at large x, and oxygen vacancies are the dominant migrating species [10,11]. $Gd_2Zr_2O_7$ has the highest intrinsic ionic conductivity ($\sim 10^{-2}$ S/cm at 1000 K) of any of the pyrochlore compounds [12], and it is comparable to that of yttria-stabilized zirconia—the electrolyte most commonly investigated for the development of solid-oxide fuel cells [13]. The substitution of Zr for Ti in the $Gd_2(Ti_{1-x}Zr_x)_2O_7$ system results in a 2-orders-of-magnitude increase in ionic conductivity in going from $Gd_2(Zr_{0.3}Ti_{0.7})_2O_7$ to $Gd_2Zr_2O_7$ [3]. This increase is related to an increase in anion disorder with increasing Zr content. The Frenkel disorder is the source of oxygen-ion conduction in the pyrochlore structure [11,14,15]. Generally, the ratio of cation-oxygen bond lengths for pyrochlores, $r_{A\text{-}O}/r_{B\text{-}O}$, is in the range of 1.10–1.24. The systematic decrease in the average A to B cation radii ratio, in the limit, leads to complete disordering of the pyrochlore structure and the defect fluorite structure $(A, B)_4O_7$ [16]. The systematic disordering of both the cation and anion sublattices with increasing x has also been confirmed by neutron scattering studies of the closely related pyrochlore, $Y_2(Ti_{1-x}Zr_x)_2O_7$ [17,18]. Static lattice energy minimization calculations [14] and molecular dynamics simulation [15] suggest that diffusion controls the ionic conductivity due to an oxygen-ion $48f$ vacancy-hopping mechanism. Furthermore, the anion vacancy migration energy is sensitive to the configuration of the cation antisite disorder, and oxygen-ion mobility decreases with cation antisite disorder [11,14,15]. The intrinsic increase in anion vacancy concentration, which is more important than the reduced oxygen ion mobility in the disordered state, leads to a large increase in ionic conductivity that is associated with a decrease in electronic conductivity.

Ionic conductors are the basis for technologies that utilize solid-state electrochemical cells as a source of clean and efficient energy, such as in high-temperature batteries and fuel cells, and as sensors [13,19,20]. Recently, nanoscale heterostructures of fast-ion conductors,

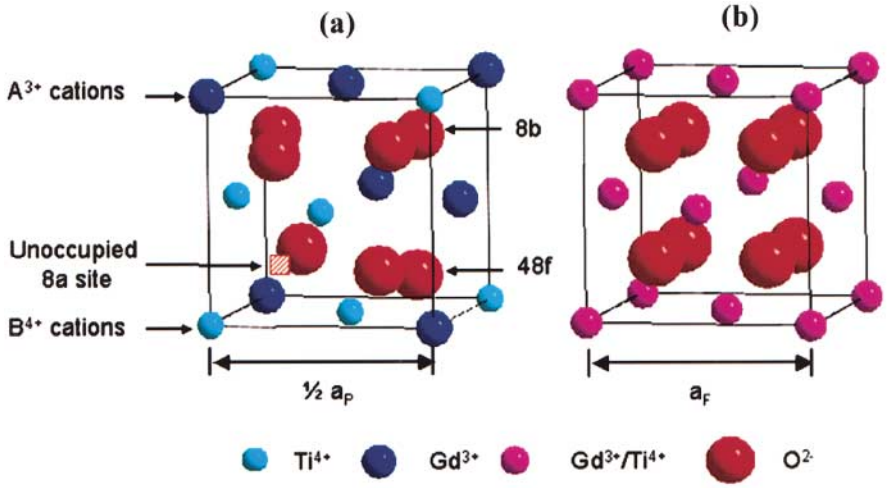

FIG. 1 (color). Structure of pyrochlore and defect fluorite. (a) Partial unit cell of the ordered pyrochlore structure. The larger A^{3+} cations are eight-coordinated and located within distorted cubic polyhedra; the smaller B^{4+} cations are six-coordinated and located in distorted octahedra. 48*f* oxygen is coordinated to two B^{4+} and two A^{3+} cations, while the 8*b* oxygen is in tetrahedral coordination with only A^{3+} cations. An unoccupied interstitial site at 8*a* is surrounded by four B^{4+} ions and the vacancies are ordered. (b) Cation and anion disordering causes the transformation of the ordered pyrochlore to a defect-fluorite structure with a halving of the isometric unit cell parameter. The occupancy for each anion site is then 0.875.

composed of CaF_2 and BaF_2, were made for the first time using molecular beam epitaxy [21]. The goal of such work has been to increase ionic conductivity by increasing either the atomic-scale structural disorder or by fabricating nanoscale geometries that increase the boundary domain surface area [21,22]. The use of "tunable" titanate mixed conductors controlled by appropriate doping [10,23,24] and the zirconate ionic conductor (electron insulator) controlled by cation disordering is of particular technological importance for applications in solid fuel cells. Ideally, one could construct a monolithic fuel cell [25] in which the electrodes and electrolyte are mechanically and chemically compatible because they are fabricated from the same pyrochlore oxide but with the variation in electronic properties arising from variations in composition and the degree of disorder.

Here we report the formation of nanoscale defect-fluorite layers (fully disordered) within pyrochlore substrates (fully ordered) by an ion-irradiation-induced order-disorder transformation. We have previously described the ion-irradiation-induced order-disorder transformation of pyrochlore in studies of $Gd_2Ti_2O_7$ [26,27]. Ion irradiations (600 keV Ar^+ at 6.5×10^{14} ions/cm^2) of $Gd_2Ti_2O_7$ indicated that the pyrochlore superstructure transforms to a defect-fluorite structure due to the cation and anion disorder induced by ion irradiation prior to complete amorphization. The $Gd_2Ti_2O_7$ structure is especially sensitive to radiation-induced amorphization [28,29], becoming amorphous at a dose of ~0.18 displacement per atom (dpa)—based on *in situ* transmission electron microscopy (TEM) observation [26]. However, the *B*-site cations play an important role in the radiation response of pyrochlores, and a systematic study of $Gd_2(Zr_xTi_{1-x})_2O_7$ showed that the radiation resistance increases with the zirconium content so that $Gd_2Zr_2O_7$ could not be amorphized at a dose of ~34 dpa (1.5 MeV Xe^+ irradiation). An ion-irradiation-induced pyrochlore-to-fluorite structure transformation was also observed in $Gd_2Zr_2O_7$ (Fig. 2). The observed extreme radiation resistance of $Gd_2Zr_2O_7$ is related to its ability to accommodate lattice disorder by cation disordering on the *A* and *B* sites [30].

Single crystals of $Gd_2Ti_2O_7$ were grown in Pt crucibles at a fixed temperature of 1235 °C by means of a technique involving the slow evaporation of a predominantly lead-fluoride-based flux. The resulting specimens were confirmed to be an ordered pyrochlore structure by selected-area electron diffraction (SAED). The 1.5 MeV Xe^+ irradiations of the single crystal $Gd_2Ti_2O_7$ were conducted at the High Voltage Electron Microscope (HVEM)-Tandem facility at Argonne National Laboratory. *Ex situ* cross-section TEM and high-resolution TEM (HRTEM) images were obtained using a JEOL 4000 EX.

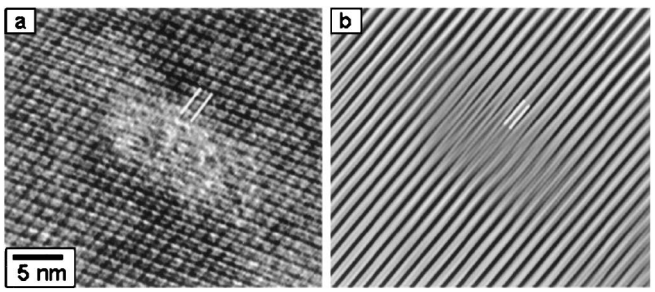

FIG. 2. Ion-irradiation-induced pyrochlore-to-fluorite structure transformation in $Gd_2Zr_2O_7$. (a) A damaged domain. (b) A Fourier-filtered image showing the fluorite lattice spacing within pyrochlore substrate. Ion irradiation-induced order-disorder transformation is evidenced by the halving of the (111) spacing as marked in the figure.

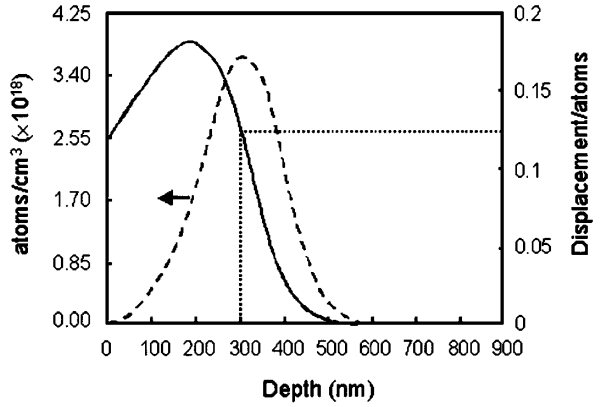

FIG. 3. Ion distribution and damage profile calculated by TRIM-96 for 1.5 MeV Xe^+ in a $Gd_2Ti_2O_7$ single crystal (ion dose: 8.55×10^{13} ions/cm^2). Ion range and peak in damage are ~297 nm and ~190 nm, respectively.

The ion distribution and damage profile in the $Gd_2Ti_2O_7$ single crystal target were simulated using the TRIM-96 code. An atomic displacement energy of 50 eV for $Gd_2Ti_2O_7$ was used. The ion range and damage peak for 1.5 MeV Xe^+ irradiation of the $Gd_2Ti_2O_7$ single crystal are ~297 nm and ~190 nm, respectively (Fig. 3). Thus, a buried amorphous layer (several nm) should be observed in the irradiated sample at an ion dose of 8.55×10^{13} ions/cm^2—the dose at which the damage exceeds that required to completely amorphize $Gd_2Ti_2O_7$ at room temperature. A cross-section transmission electron microscopy image (Fig. 4) indicated that a completely amorphous layer was produced near the surface, and its depth (~300 nm) is in good agreement with the range calculated using TRIM-96. Below the amorphous layer, however, there is a mixed domain of pyrochlore and fluorite structure types, as indicated by the SAED patterns. The pyrochlore and fluorite structures can be distinguished by the presence or absence of superlattice diffraction maxima (weak diffraction spots in SAED). The critical dose required to completely amorphize a single crystal of $Gd_2Ti_2O_7$ is ~0.13 dpa.

A continuous layer with the disordered fluorite structure within an ordered pyrochlore substrate was created by 1.5 MeV Xe^+ irradiation of a single crystal of $Gd_2Ti_2O_7$ at a dose (8.55×10^{12} ions/cm^2) less than the critical amorphization dose. This buried defect-fluorite layer (Fig. 5) (~12 nm thick) occurs at a depth of ~190 nm, corresponding to the calculated peak in damage (Fig. 3). In contrast to the pyrochlore substrate, the lattice constant of the buried fluorite-structure layer is one-half that of the pyrochlore substrate, as shown by the difference of the (111) spacing (Fig. 5). To confirm the formation of the defect-fluorite structure in the buried layer, HRTEM image simulations were completed. The simulated image (Fig. 6a) shows good agreement with the actual image (Fig. 5; see the 4×4 unit cells in the rectangular inset in the pyrochlore substrate). Figure 6a (right side) provides the schematic representation of the structure used for the image simulation. The superstructure image was obtained for a defocus value of 15 nm and a thickness of 2 nm. The simulated image confirms that the phase contrast of the superstructure is mainly formed by the cations. In the simulation of the image for the disordered cation and anion sublattices (which are based on the defect-fluorite structure), the superstructure disappears at the same defocus and thickness values (Fig. 6b). The simulated image corresponds to the rectangular area (8×8 cells) shown in the inset in the buried layer (Fig. 4). Thus, the buried defect-fluorite layer is caused by the

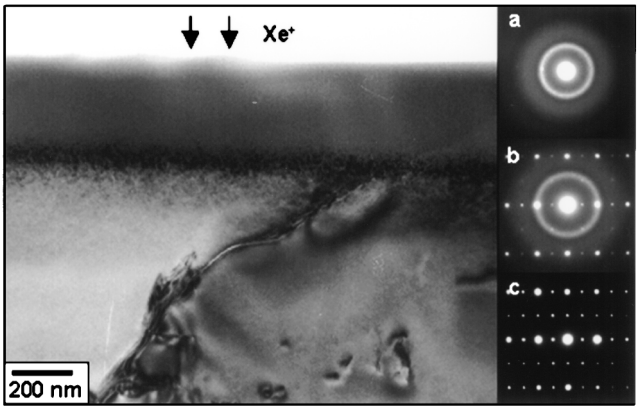

FIG. 4. Cross-section TEM image of a $Gd_2Ti_2O_7$ single crystal irradiated by 1.5 MeV Xe^+ at an ion dose of 8.55×10^{13} ions/cm^2 (amorphous layer thickness ~300 nm). (a) SAED pattern from an amorphous layer. (b) SAED pattern from a highly damaged layer consisting of a mixed domain of pyrochlore and fluorite. (c) SAED pattern from a pyrochlore substrate. The critical amorphization dose for $Gd_2Ti_2O_7$ is ~0.13 dpa based on the thickness of the amorphous layer from Fig. 2.

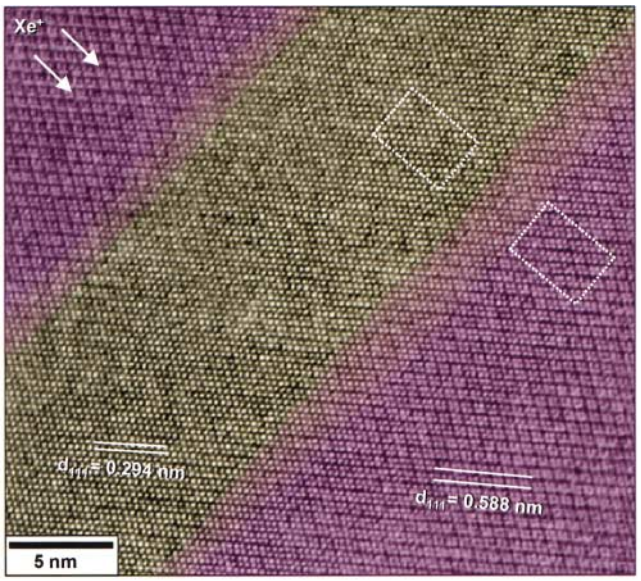

FIG. 5 (color). High-resolution TEM image showing the continuous buried defect-fluorite layer (green) within the ordered pyrochlore substrate (purple). The thickness of the buried layer is ~12 nm. The two inset rectangles represent the areas used for the computer simulations shown in Fig. 6.

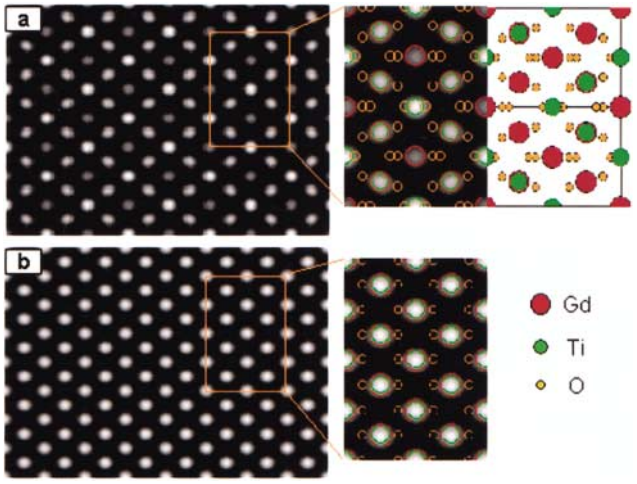

FIG. 6 (color). Computer simulation of HRTEM images of the [011] zone axis of ordered pyrochlore and defect fluorite. (a) Simulated image showing the superstructure (4×4 unit cells) outlined by the rectangular inset in the pyrochlore substrate (purple) in Fig. 5. The atom overlay (upper right-hand corner) shows the structure model used for the image simulation and the contribution of cations and anions to the simulated image contrast. (b) Simulated image (8×8 unit cells) corresponding to the rectangular inset in the buried layer (green) in Fig. 5 shows the loss of superstructure in the defect-fluorite layer.

cation and anion disordering induced at the peak of the ballistic interactions between the ion and target atoms. The radiation required to cause the pyrochlore-fluorite transformation in $Gd_2Ti_2O_7$ pyrochlore was determined to be $\sim$0.017 dpa based on the width of the buried layer. Note that the boundary between the fluorite-structure and pyrochlore-structure regions is coherent with no evidence of lattice strain.

The development of mixed ionic and electronic conducting ceramic oxide membranes for oxygen separation in fuel cells is an essential element in the development of solid oxide fuel cells. In this example, we have demonstrated the successful change in the structure and geometry required to manipulate the electronic and ionic conduction properties of pyrochlore by the formation of a nanoscale, buried fluorite layer by an ion-irradiation-induced order-disorder transformation. The boundary between the fluorite- and pyrochlore-structure layers is a perfect lattice match comparable to that obtained by thin-film epitaxial methods. Ion-beam irradiation offers a method for precisely controlling the depth and width of the buried layer by varying the energy and mass of implanted ions. Further flexibility in the composition and degree of disorder in the nanodomains can be obtained by combining radiation-induced disorder with ion-beam implantation (Zr implanted into the $Gd_2Ti_2O_7$) and subsequent thermal treatments. The present results establish that by combining ion-beam-induced order-disorder transformations and changes in composition due to the implantation of dopant ions one can effectively design and fabricate new nanoscale mixed ionic-electronic conductors in the family of pyrochlore oxides.

This work was supported by Division of Materials Science of the Office of Basic Energy Sciences of the U.S. Department of Energy, through Grant No. DE-FG02-97ER45656. We are also grateful for the support of the technical staff at the HVEM-Tandem Facility at Argonne National Laboratory.

*Email address: rodewing@umich.edu

[1] M. A. Subramanian, G. Aravamudan, and G. V. S. Rao, Prog. Solid State Chem. **15**, 55 (1983).
[2] B. C. Chakoumakos, J. Solid State Chem. **53**, 120 (1984).
[3] P. K. Moon and H. L. Tuller, Solid State Ion. **28–30**, 470 (1988).
[4] B. J. Wuensch and K. W. Eberman, JOM **52**, 19 (2000).
[5] S. Meilicke and S. Haile, Mater. Res. Soc. Symp. Proc. **393**, 55 (1995).
[6] P. K. Moon and H. L. Tuller, Sens. Actuators B **1**, 199 (1990).
[7] H. L. Tuller, Solid State Ion. **52**, 135 (1992).
[8] B. J. Wuensch *et al.,* Solid State Ion. **129**, 111 (2000).
[9] S. A. Kramer and H. L. Tuller, Solid State Ion. **82**, 15 (1995).
[10] S. Kramer, M. Spears, and H. L. Tuller, Solid State Ion. **72**, 59 (1994).
[11] R. E. Williford, W. J. Weber, R. Devanathan, and J. D. Gale, J. Electroceram. **3**, 409 (1999).
[12] A. J. Burggraaf, T. Van Dijk, and M. J. Verkerk, Solid State Ion. **5**, 519 (1981).
[13] J. B. Goodenough, Nature (London) **404**, 821 (2000).
[14] P. J. Wilde and C. R. A. Catlow, Solid State Ion. **112**, 173 (1998).
[15] P. J. Wilde and C. R. A. Catlow, Solid State Ion. **112**, 185 (1998).
[16] P. K. Moon and H. L. Tuller, Mater. Res. Soc. Symp. Proc. **135**, 149 (1989).
[17] C. Heremans, B. J. Wuensch, J. K. Stalick, and E. Prince, J. Solid State Chem. **117**, 108 (1995).
[18] O. Knop, F. Brisse, and L. Castelliz, Can. J. Chem. **47**, 971 (1969).
[19] A. V. Chadwick, Nature (London) **408**, 925 (2000).
[20] P. Lacorre, F. Goutenoire, O. Bohnke, R. Retoux, and Y. Laligant, Nature (London) **404**, 856 (2000).
[21] N. Sata, K. Eberman, K. Eberl, and J. Maier, Nature (London) **408**, 946 (2000).
[22] H. L. Tuller, J. Electroceram. **1**, 211 (1997).
[23] O. Porat, C. Heremans, and H. L. Tuller, Solid State Ion. **94**, 75 (1997).
[24] H. L. Tuller, Solid State Ion. **94**, 63 (1997).
[25] H. L. Tuller, in *High Temperature Electrochemistry: Ceramics and Metals,* edited by F. W. Poulsen *et al.* (Risø National Laboratory, Roskilde, Denmark, 1996), p. 139.
[26] S. X. Wang, L. M. Wang, R. C. Ewing, G. S. Was, and G. R. Lumpkin, Nucl. Instrum. Methods Phys. Res., Sect. B **148**, 704 (1999).
[27] S. X. Wang *et al.,* J. Mater. Res. **14**, 4470 (1999).
[28] W. J. Weber, J. W. Wald, and Hj. Matzke, J. Nucl. Mater. **138**, 196 (1986).
[29] W. J. Weber and R. C. Ewing, Science **289**, 2051 (2000).
[30] K. E. Sickafus *et al.,* Science **289**, 748 (2000).